Astron. Astrophys. 96, 164–173 (1981)

ASTRONOMY AND ASTROPHYSICS

Formation and Properties of Persisting Stellar Bars

F. Combes[1] and R. H. Sanders[2]

[1] Ecole Normale Supérieure (ERA 762), Paris et Observatoire de Paris-Meudon, F-92190 Meudon, France
[2] Kapteyn Laboratory, Groningen, The Netherlands

Received February 21, accepted July 22, 1980

Summary. Long time-scale three dimensional N-body simulations of galaxies composed of two components, a self-consistent disk and a spheroidal halo, demonstrate that bars develop over a large range of halo mass to disk mass ratio (M_h/M_d). Such non axisymmetric systems dynamically evolve at a rate which depends upon M_h/M_d. For systems with low mass haloes ($M_h/M_d \leqq 1$), strong bars quickly form but then weaken to a quasi steady state in less than twenty rotation times. For systems with high halo mass, the bar strength is still increasing after 20 rotation times. This suggests that the strong bars observed in SBb galaxies have not persisted since the epoch of galaxy formation but have developed more recently in systems with $M_h/M_d \geqq 2$.

Key words: galactic structure – star – stellar dynamics

I. Introduction

The presence of barred structure seems to be a very general attribute of disk galaxies. Perhaps half of all spirals should be classified as barred or intermediate barred (de Vaucouleurs, 1963). This high frequency of occurrence and the fact that bars (at least in early-type systems) consist of an old stellar population, suggest that bars are long-lived and fundamental components of the mass distributions of disk systems. Moreover, there is evidence that some galaxies contain bars which represent very strong deviations from axial symmetry. This conclusion is based on a comparison of gas dynamical calculations with the observed gas distributions and motions in SBb systems (Sanders and Tubbs, 1980). These calculations imply that the bars in such galaxies have the following characteristics:

1. they are strong, with the maximum tangential force exceeding 30% of the local axisymmetric force.

2. they cannot be represented by a single $m=2$ distorsion of a disk. Higher order harmonics must be present in a Fourier expansion of mass or potential distribution.

3. the overall mass distribution must be centrally condensed with present respect to the bar. The bar extends beyond the peak in the rotation curve of an axially symmetrized mass distribution.

4. such bars must be rotating rather rapidly, with corotation at a radius which is not more than twice the radius of the maximum tangential force due to the bar.

Numerical and analytical calculations during the past decade have established that cold self-gravitating disks are unstable to the formation of bars (Hohl and Hockney, 1969; Miller et al., 1970; Kalnajs, 1972; James and Sellwood, 1978). Bars generated in numerical experiments form in one or two rotation times but then seem to weaken over several additional rotation times (see Hohl, 1975), i.e. there is a suggestion of continuing dynamical evolution of these non-axisymmetric systems in a time scale longer than a rotation or dynamical time scale. Indeed, recent 3 D calculations by Hohl and Zang (1979) demonstrate very clearly that systems with bars are continuing to dynamically evolve after five rotation times. Therefore it is reasonable to ask how strong bars evolve in disk systems.

It is well known that the presence of a hot spheroidal halo affects the overall stability of the disk against bar forming modes (Ostriker and Peebles, 1973). This suggests that the presence of a halo would have significant influence on the growth and evolution of bars. We investigate this possibility in the present paper by means of numerical N-body calculations. We follow the time evolution of several disk systems embedded in rigid haloes. The free parameter in these calculations is the halo mass to disk mass ratio. The essential difference between the present and previous numerical calculations is the length of time over which galactic evolution is followed. In four cases we numerically follow the evolution for 20 rotation time scales or about $5\ 10^9$ yr. This is done because the essential question which we investigate is the influence of the halo on the long-term evolution of the bar phenomenon. In addition we determine the dynamical characteristics of long-lived bars (strength, angular velocity, degree of central concentration, presence of resonances), and we compare these results with the models required to excite the observed gas response in SBb galaxies (Sanders and Tubbs, 1980).

II. The Physical Model

Galactic disks embedded in spherical haloes are simulated by three-dimensional (3 D) N-body calculations. The model galaxy is composed of two components: a three dimensional disk of 16,000 mass points, representing the flattened star population, and a spherically symmetric and more centrally concentrated rigid component representing a bulge-halo. Initially, both disk and halo have a potential of the form (cf. Toomre, 1963):

$$\phi = \phi_0 (1 + r^2/a^2)^{-1/2} \quad (1)$$

where a is the radial scale length of a given component (a_d and a_h for disk and halo respectively). Therefore, there are two dimensionless free parameters in our model, the ratios of radial scale lengths and the ratio of disk to halo masses: a_h/a_d and M_h/M_d. In the present calculations, only the mass ratio is varied. Below we consider the initial properties of the disk and halo:

Send offprint requests to: F. Combes (Meudon)

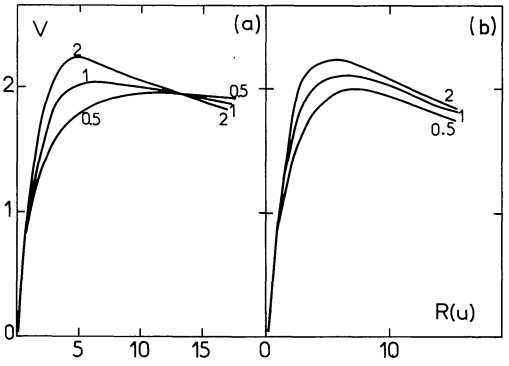

Fig. 1. Initial rotation curves for three of the simulated models. Curves are labelled by the halo-to-disk mass ratio. The actual initial rotation curves b), are very similar to the theoretical curves a), the difference comes mainly from the truncation of the disk. The unit of length may be taken as 1 kpc, so that the velocity unit is 100 km s^{-1}

Disk Component

Particles in the disk are randomly distributed such that their surface density follows the radial low of a truncated Toomre disk,

$$\mu=\mu_0(1+r^2/a_d^2)^{-3/2} \qquad r<r_d \tag{2}$$

where r_d is the maximum radius of the disk. The surface density at the origin μ_0, is determined by fixing the total mass M_d of the disk inside the radius r_d. The distribution in the z-direction has the following dependence at each radius r:

$$\varrho(r, z)=\varrho(r, 0)\ \mathrm{sech}^2\ (z/h(r)) \tag{3}$$

where $h(r)$ is the scale height in the z-direction

$$h(r)=h_0(1-r^2/r_d^2)^{1/2}. \tag{4}$$

The scale height in the central region h_0 is typically 1 kpc or $0.06\ r_d$. The Z distribution is truncated at the limits of the grid and is normalized according to the radial distribution of the surface density (Eq. 2). This z-exponential law corresponds to the equilibrium distribution of a one dimensional plane parallel system (cf. Spitzer, 1968).

Initially, particles are given a systematic tangential velocity. There are no radial or z-velocities and the tangential velocity dispersion is zero; therefore, the disk is completely cold in the sense of Ostriker and Peebles (1973). The actual initial rotation curve for the ensemble of particles which is computed by the model is not very different from that of the untruncated Toomre disk (Fig. 1). The discrepancy is due primarily to the truncation of the disk and to a lesser extent to a non-Newtonian force law at distances less than about one or two cell-lengths. When M_h/M_d is high, these two effects are smeared out by the presence of the halo, whose potential is computed exactly and which is not truncated.

In a few test runs the particles were given an initial random motion sufficient to prevent local axisymmetric instabilities (Toomre, 1964). After one or two dynamical times the behavior of those initially warm systems was identical to the initially completely cold systems, due to the overwhelming importance of non-axisymmetric modes in relaxing the systems.

Any choice of initial conditions for the disk is, of course, arbitrary; however, since galactic disks presumably form by dissipationnal collapse of a gas cloud with high specific angular momentum (cf. Eggen et al., 1962), it is expected that disks may initially be rather cold.

Halo

This is the spherical and centrally condensed rigid potential included to stabilize or partially stabilize, the disk. The stabilizing effect is the same when this halo-component is made self-consistent, as shown by Hohl (1978). The potential of the halo [cf. Eq. (1)], is normalized such that the halo mass interior to the radius r_d is M_h. The quantity M_h/M_d is the ratio of halo to disk mass inside the same radius r_d.

The chosen halo potential (1) leads to a density distribution:

$$\varrho_h(r)=\varrho_0(1+r^2/a_h^2)^{-5/2}.$$

The ratio of halo to disk length scales (a_h/a_d) is chosen to be 0.25 and is not varied. This assumes that the halo should be identified with the observed bulges in spiral galaxies (the halo is the extension of the bulge) and therefore, this spheroidal component is distinct from proposed massive extensive haloes providing flat rotation curves at large radii (Ostriker et al., 1974). Such extensive haloes would have little dynamical effect in the inner regions of the galaxies considered here.

III. Technique

In our 3 D N-body calculations, the gravitational potential is obtained by the rapid Fourier transform method (see e. g. Hohl and Hockney, 1969). At each integration step, density is computed at each point of a grid of $32\times32\times16$ cells: each particle contributes to the density of the eight nearest grid points, according to the well-known CIC procedure (Birdsall and Fuss, 1969). Fourier transforms of density and potential are then carried out on a $64\times64\times32$ grid. The potential function between two particles is the Newtonian law (r^{-1}), but with a cut off at short distances and at distances larger than the total grid which contains the galaxy. The fact that the potential for distances less than one cell is taken as constant, suppresses violent close encounters and simulates a galaxy with a realistically long two-body relaxation time (see Hohl, 1973; Combes, 1980). The interaction between periodically reproduced images is avoided in the usual way (Hohl and Hockney, 1969). The force acting on each particle is computed from the gravitational potential of the nearest grid points. To avoid the excitation of the 4-fold symmetrical mode in computing the potential in a cube, only particles interior to the largest cylinder inscribed in the grid are taken into account (cf. Hohl, 1972). The particles which pass outside this boundary are advanced according to a Keplerian approximation of the force corresponding to the total interior mass.

The time step Δt is chosen to satisfy the relation:

$$V_{\max}\Delta t\lesssim L \tag{5}$$

where $V_{\max}$ is the maximum of the rotation curve and L is the cell length in the plane of the galaxy. This means that particles cannot jump more than one cell in one time step. According to this constraint, a rotation time (defined at $r=0.5\ r_d$) contains about 50 time steps in all our runs. This constraint (5) gives also a computational lower limit to the radial scale length of the halo: for a given halo mass, the computation time becomes prohibitively long if $a_h<3\ L$.

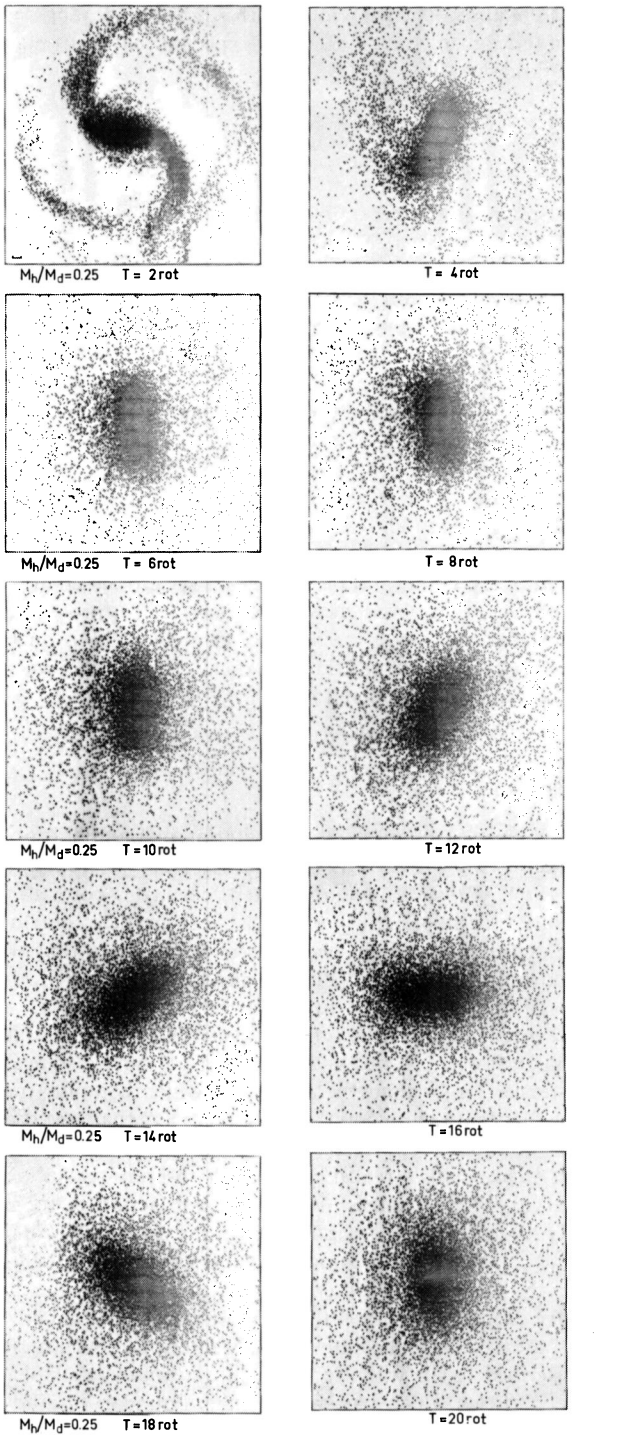

Fig. 2

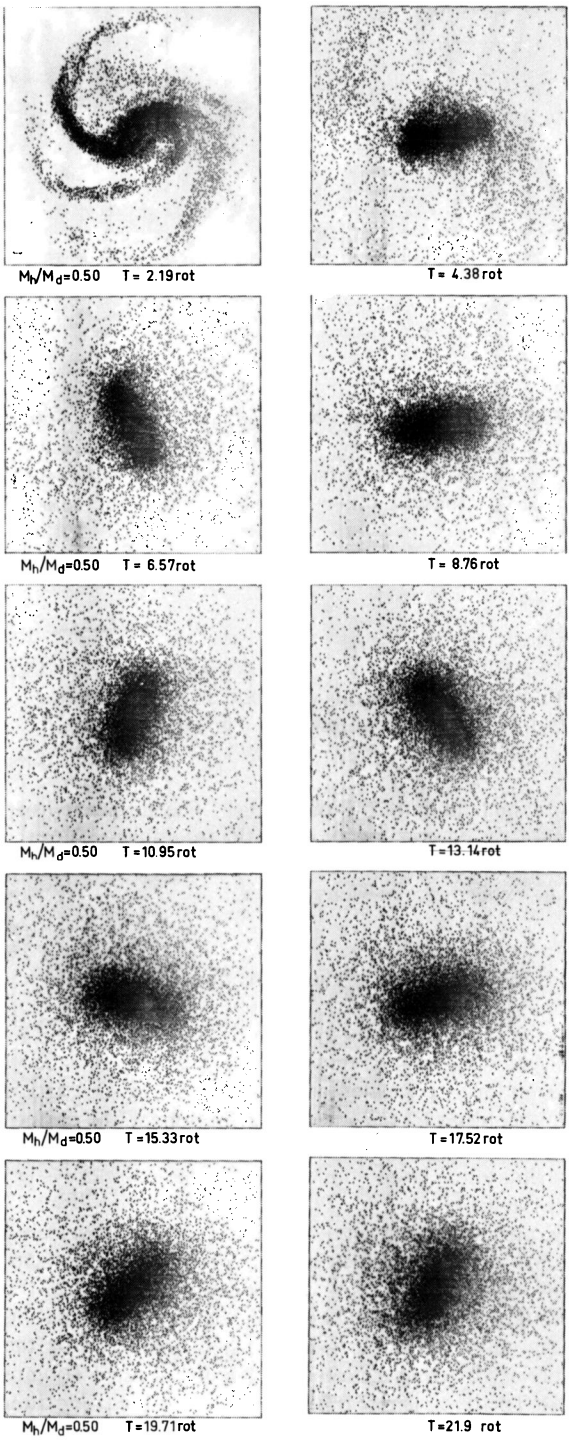

Fig. 3

Figs. 2–5. Particle plots of the four runs at various epochs: $M_h/M_d = 0.25$, 0.5, 1.0, and 2.0. A cell length is indicated by tick marks. In the first two cases, the disk radius (r_d) was half the grid radius

IV. Results of Experiments

Four cases with different ratios of halo to disk masses were run with the same ratio a_h/a_d (0.25). For these four cases, the ratio M_h/M_d was 0.25, 0.5, 1.0, 2.

The cases $M_h/M_d = 1, 2$ were run with the disc of particles filling the computational grid. The number of escaped particles, i.e. particles advanced only approximately, was always under 15%. The number of escaped particles increases very quickly as the halo mass decreases, since the disk then undergoes more violent

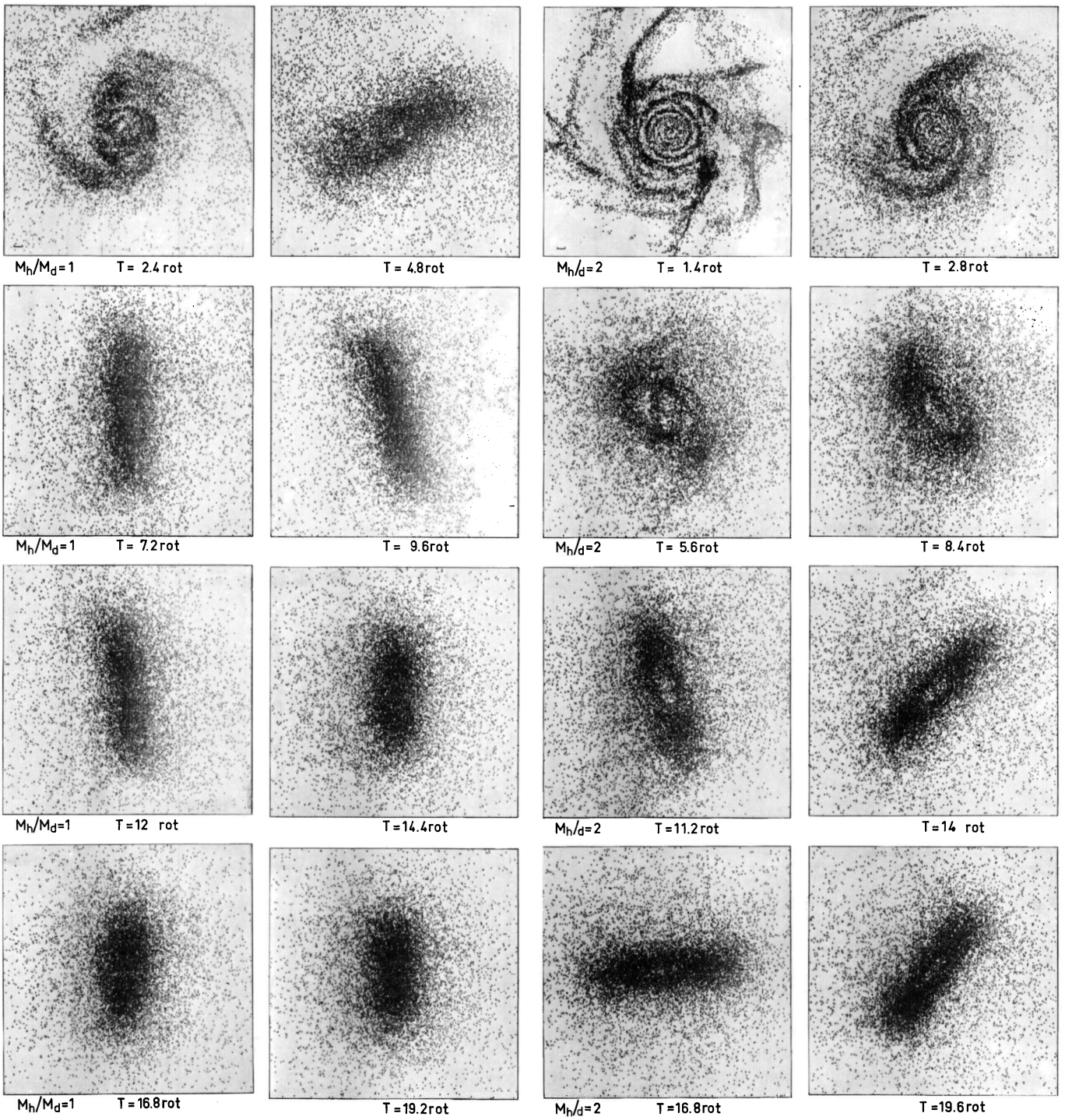

Fig. 4.

Fig. 5.

instabilities. For the $M_h/M_d = 0.25$ and 0.5 cases, the large number of escaped particles leads us to reduce the radius of the disk in units of the grid cell length, by a factor of 2, so that the number of escaped particles was reduced below 20%. A test run for the case $M_h/M_d = 1$ was carried out with the reduced grid radius and this run was identical to the run in which the disk fills the grid; therefore a finer scale is justified in the large M_h/M_d cases.

If the unit of length in the calculations is assumed to be 1 kpc (the initial disk has a maximum radius of 16 kpc), and the total mass of the galaxy (halo and disk inside 16 kpc) is taken to be $10^{11}\,M_\odot$, then the maximum rotational velocity is about 220 km s^{-1}. Then condition (5) requires a time step of about $5\,10^6$ yr. One rotation time at the half-grid radius ($r_{\frac{1}{2}} = 8$ kpc) is typically $2.5\,10^8$ yr. Since all cases were run for 20 rotation times, this

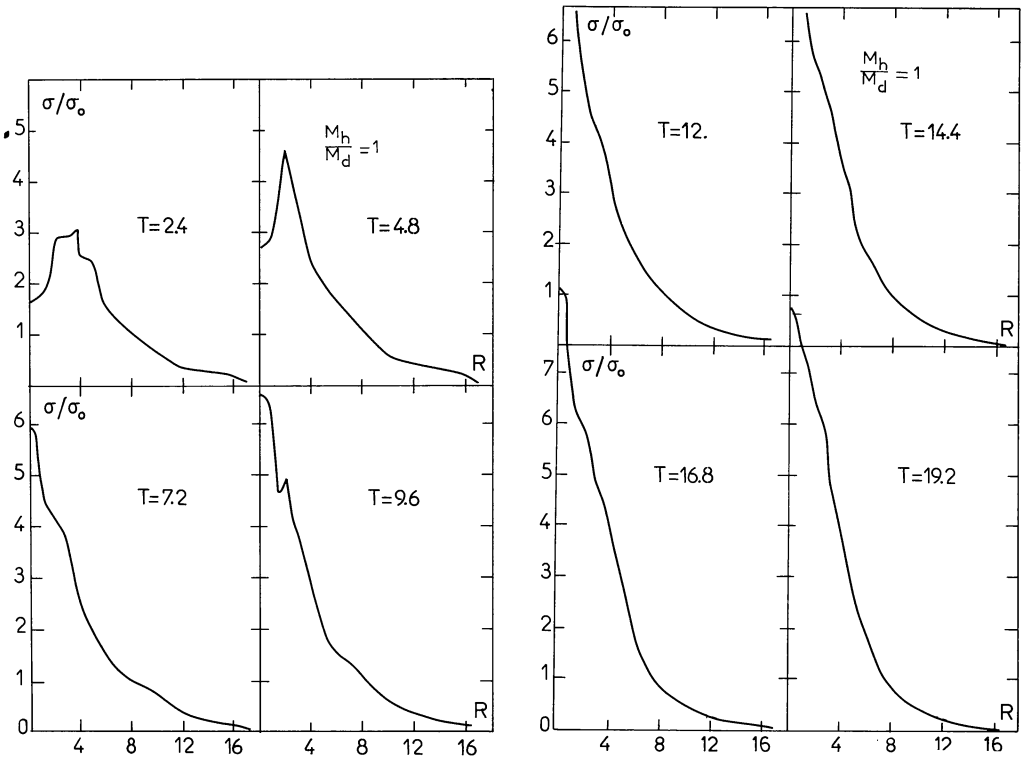

Fig. 6. Evolution of surface density distribution for the model $M_h/M_d=1$

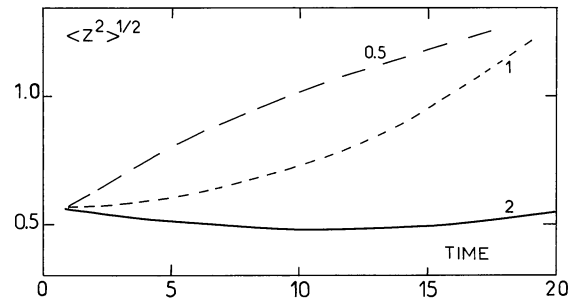

Fig. 7. Mean thickness of the galaxy disks as a function of time

corresponds to a total physical time scale of $5\,10^9$ yr for the simulations.

The results are shown in Figs. 2–5. These are particle plots viewed perpendicular to the plane of the disk, at successive epochs; the time is reckoned in rotation time at the radius $r=0.5\,r_d$ for each case. Pictures are shown more frequently at the beginning of the runs when the evolution is faster. In all cases bars are seen to develop from an apparent $m=2$ instability. The growth time scale of the bar increases with M_h/M_d which is consistent with previous results (Hockney and Brownrigg, 1974; Miller, 1978). In all the cases, bars are seen to persist for 20 rotation times. We can see for the case $M_h/M_d=2$, there develops a small hole in the central density. This may be due to the fact that particles in the central cells tend to move radially outward due to their high centrifugal forces that cannot be exactly balanced by the model.

The evolution of the radial distribution of the surface density is also more rapid when the halo is less massive. The case of $M_h/M_d=1$ is shown in Fig. 6. It is seen that particles tend to gather in the center and to evolve towards an exponential radial

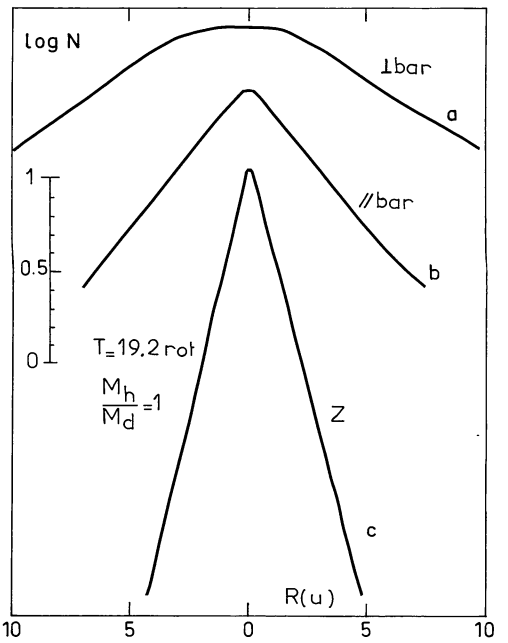

Fig. 8. Density profiles across the bar for the case $M_h/M_d=1$ and $T=19.2$ rotations, when the galaxy is seen edge-on: a) strip along the plane ($z=0$), along the larger length of the bar, and b) along the smaller length of the bar, c) strip perpendicular to the plane, when the galaxy exhibits the perpendicular box shape (smaller section of the bar)

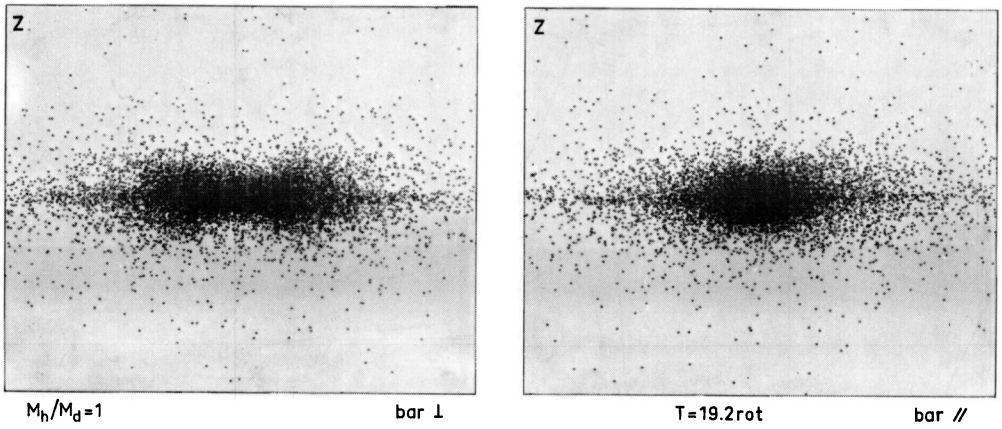

Fig. 9. Edge-on views of the bar, for the case $M_h/M_d=1$, at the end of the simulation. Note the box shape morphology of the galaxy in the view perpendicular to the major axis of the bar

distribution. In this case, the maximum surface density doubles in ten rotations, but then does not increase over the final 10 rotations, indicating that a steady-state has been reached. This behavior is similar to that found in earlier experiments (cf. Hohl, 1972, Miller and Smith, 1979). For the other values of M_h/M_d, the behaviour of surface density distribution is similar apart from the time scales.

The mean thickness of the disks as a function of time is displayed in Fig. 7, for three cases of M_h/M_d. In all cases, the thickness is increasing, but this increase is only very slight in the case $M_h/M_d=2$. This behaviour, which was also detected by Hohl (1978), is probably related to the stabilizing effect of the halo.

In all cases, bars appear relatively narrow. The axial ratios in the plane range from 2 to 3. In Fig. 8, are shown density profiles along and across the bar for the case $M_h/M_d=1$, $T=7.2$ rotations. It is interesting to note the peculiar morphology of a barred galaxy, when viewed edge-on. In Fig. 9 we see the case $M_h/M_d=1$, at the end of the simulation ($T=19.2$ rot.). Similar shapes occur in all other cases. In a view where the galaxy is edge-on and the line of sight is parallel to the long axis of the bar, the system looks like a box (to be compared to NGC 7332); and in a view where the line of sight is perpendicular to the long axis of the bar (Fig. 9), it is easy to recognize a peanut-shape morphology, very similar to the edge-on S 0 galaxy NGC 128 (Hubble Atlas, Sandage, 1961). From the computation of the z-oscillation frequency of the particles as a function of radius ($\nu_z(r)$), it is found that there exist high order resonances between the bar motion and the z-motions of the particles; in particular, the 4$^{\text{th}}$ order resonance ($\Omega_b=\Omega-\nu_z/4$), always occurs at the radius of highest thickness of the peanut shape. The peculiar shapes occurring in NGC 128 and in other galaxies (see Freeman, 1977), can thus be a consequence of the presence of a bar.

V. Analysis of Results

A) Definitions

To quantitatively follow the formation and evolution of a bar, it is useful to compute the Fourier transform of the potential of the system in polar coordinates. We may write the potential, in the plane of the galaxy ($z=0$), as:

$$\Phi(r,\varphi)=\Phi_0(r)+\sum_m \Phi_m(r)\cos\left[m(\varphi-\varphi_m)\right]. \tag{6}$$

It is convenient to represent each amplitude by the corresponding ratio Q_m,

$$Q_m(r)=-m\Phi m/r\,\frac{\partial\Phi_0}{\partial r} \tag{7}$$

which is the amplitude of the m^{th} harmonic in terms of the mean axisymmetric force. We also define Q_t as:

$$Q_t(r)=\partial\Phi/\partial\varphi\Big)_{\max}\Big/\,r\,\frac{\partial\Phi_0}{\partial r}. \tag{8}$$

This quantity, the maximum tangential force in terms of the mean radial force, is a measure of the strength of the bar. The variation of the phase φ_m with radius, discriminates between bars and spiral arms; for instance, in a bar-like potential, the phase φ_2 is the same at all radii. The quantity $\partial\varphi_2/\partial t$ is the angular velocity of the pattern, Ω_p.

For bar distortion of a disk there exist resonances which are identical to the Lindblad resonances discussed for spiral structure. An essential dynamical property is the number of resonances implied by the angular velocity of the pattern Ω_p. The zero$^{\text{th}}$ order epicyclic frequency k

$$k=\left(3\Omega^2+\frac{\partial^2\Phi_0}{\partial r^2}\right)^{1/2} \tag{9}$$

and the critical frequencies $\Omega+k/2$ and $\Omega-k/2$ are evaluated in these calculations as a function of radius.

A basic dynamical property of N-body systems is the relative energy in systematic bulk motions. A convenient measure of this property is the ratio of mean ordered kinetic energy to total potential energy; i.e.

$$t=\frac{T_{\text{bulk}}}{|W|}.$$

This parameter seems to be related to the stability of the system against bar forming modes (see Ostriker and Peebles, 1973). We determine this parameter for our models by first computing the kinetic energy in systematic motions:

$$T_{\text{bulk}}=\frac{1}{2}m\sum_{i=1}^{N}V_i^2$$

where m is the mass of each particle and V_i is the average stream velocity at the position of the i^{th} particle. The mean stream ve-

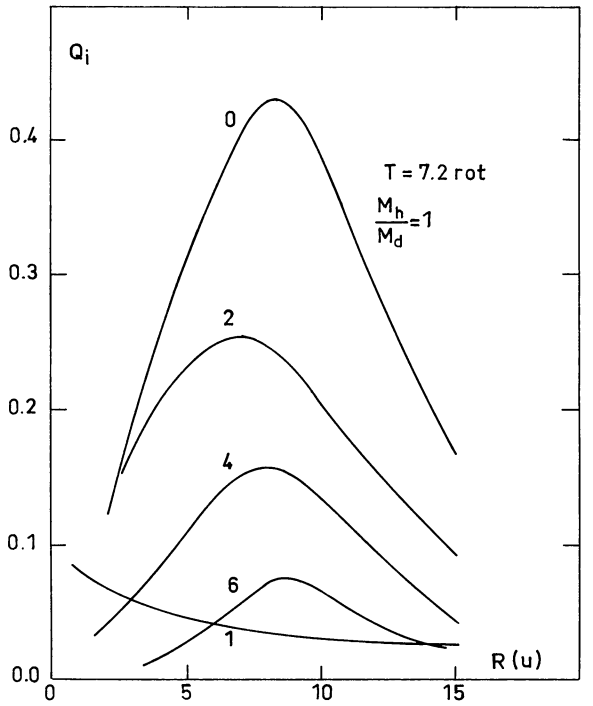

Fig. 10. Fourier analysis of the bar potential on the $Z=0$ plane. The ratio Q_i of tangential forces to the radial axisymmetric force for harmonics $i=1, 2, 4, 6, 8$ are plotted as a function of radius for $M_h/M_d=1$ at $T=7.2$ rotations. The total tangential force Qt (code 0) is also shown

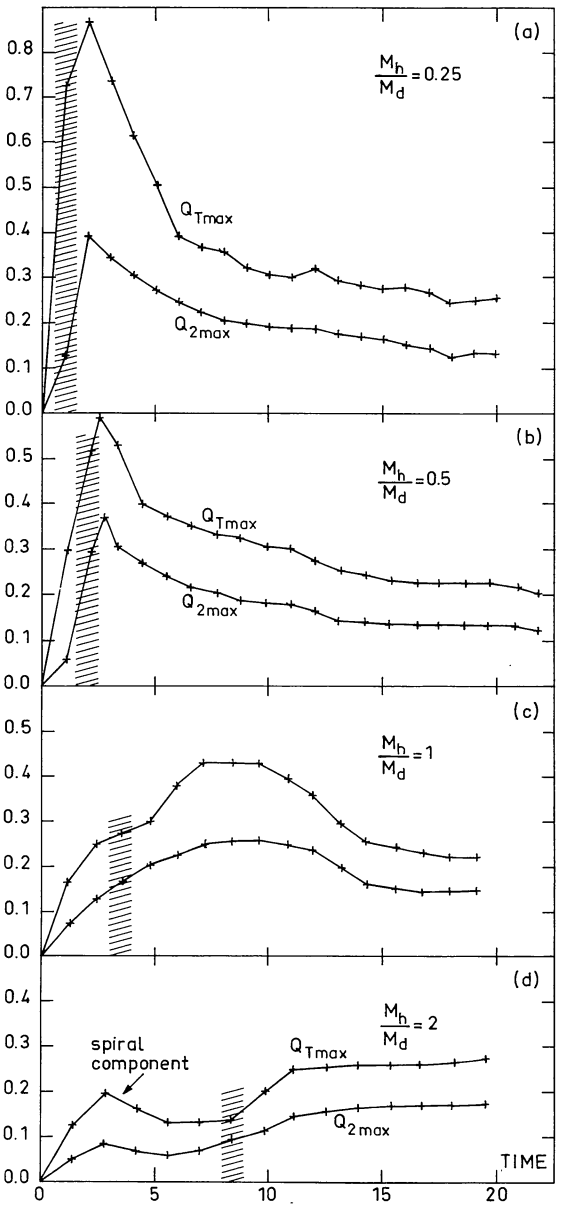

Fig. 11. Evolution of the strength of the bar perturbation as a function of time (represented by Qt_{max} and Q_2max) for the four cases. Shaded regions indicate the period of bar formation

locity is computed by averaging over the velocities of all particles within one or two cell lengths depending upon the distance to the center; i.e. the size of the averaging box regularly increases from center to periphery to include reasonable numbers of particles per averaging box. Because the halo is considered to have no systematic motion, this parameter applies to the entire system, halo plus disk. We also evaluate t_d, the ratio of mean ordered kinetic energy, to twice the total kinetic energy in the disk alone, in the absence of a halo, $t_d=t$. In other words, t_d would be the value of t measured by an observer who does not know about the existence of a halo. When the parameters t and t_d reach a stable value, the system may be considered to be in a quasi-stationary state.

For a system in equilibrium, the Virial theorem should be verified. Here, since the potential is not computed exactly, essentially because of the cut-off at small distances, the theorem is not expected to be verified exactly. We found a departure of about 15% for the flattened and self-consistent component of our models. The underestimate of potential leads then to an estimate of t which is accurate within only 15%.

B) Analysis

First we consider the Fourier analysis of the tangential force at one epoch of the simulations $M_h/M_d=1$. The quantities Q_t and Q_m ($m=1, 2, 4, 6, 8$) are shown in Fig. 10 as a function of radius at $t=7.2$ rotations. As is obvious from Fig. 4, the bar has become well-developed by this time. It is seen that the bar is quite strong with a maximum tangential force of 43% of the mean axisymmetric force at a radius (r_{max}) of 9 units (i.e. $Qt_{max}=0.43$).

The dominant Fourier component is $m=2$, but higher order components also make a significant contribution to the force. The ratio Q_{tmax}/Q_{2max} is a measure of the contribution of higher order harmonics to the tangential force, and in this case is

$$Q_{tmax}/Q_{2max}=1.7.$$

The phases of all even Fourier components do not vary with radius (within 1%), thus the potential is created by a true bar pattern. The first order Fourier component of the tangential force (Q_1) is small but non zero over the grid. The phase of this component, however, varies randomly with radius and suggests that the $m=1$ term is an artifact of statistical fluctuation in the particle density.

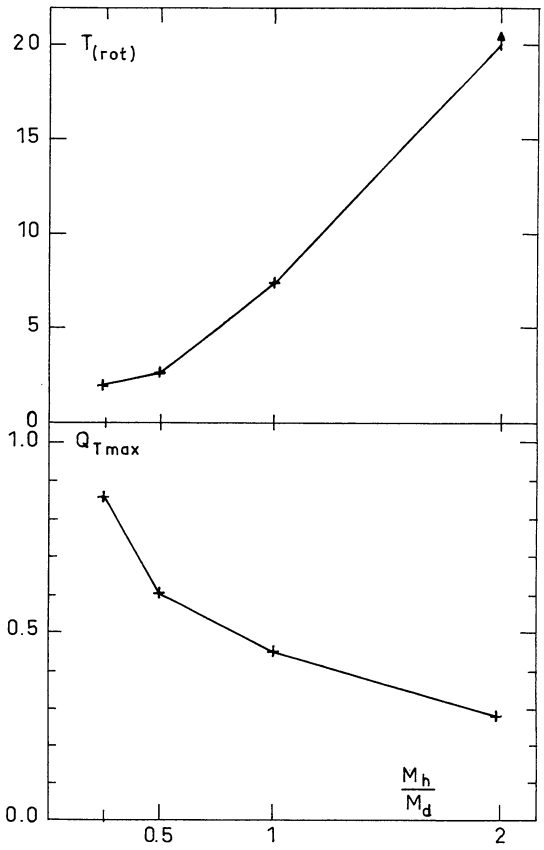

Fig. 12. a Plot of the peak strength of the bar (Qt_{max} and $Q2_{max}$) as a function of the halo-to-disk mass ratio (M_h/M_d). **b** Plot of the growth time of the bar for all cases

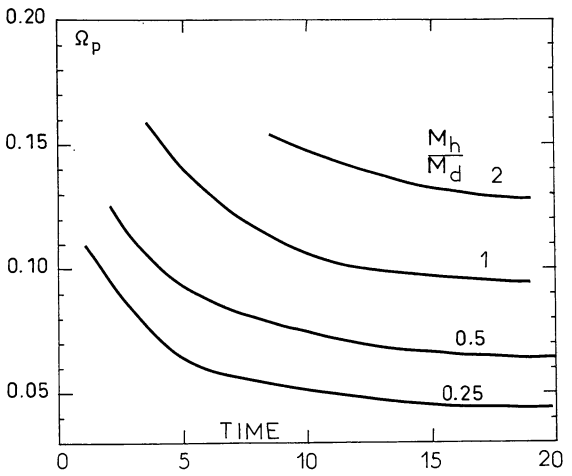

Fig. 13. Evolution of the pattern angular velocities for all cases. With standard units (see caption to Fig. 1) the unit of Ω_p is 100 km s/kpc

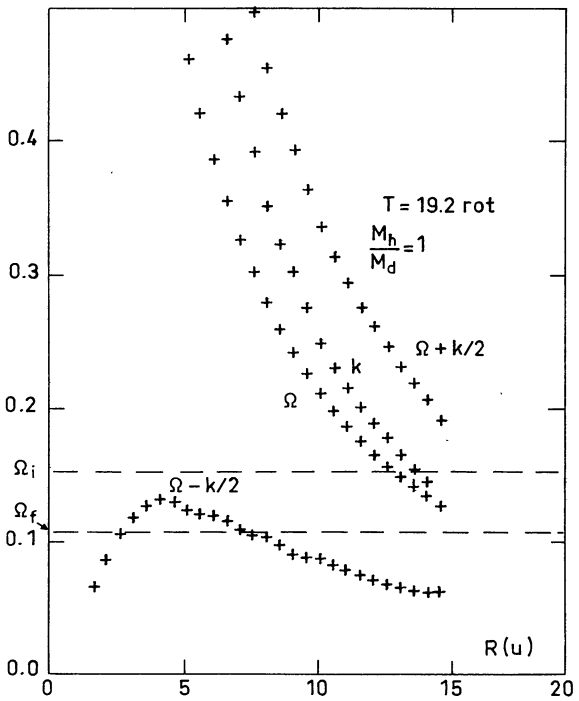

Fig. 14. The initial and final angular velocities of the bar perturbation are compared to the disk frequencies k, Ω, $\Omega-k/2$, and $\Omega+k/2$ for the case $M_h/M_d=1$

The time evolution of the bar strength for the four cases ($M_h/M_d=0.25$, 0.5, 1, 2) is shown in Fig. 11. This is a plot of the maximum values of Q_t and Q_2 as a function of time. The period of bar development is indicated by the hatched lines and it is seen that the bar develops later for greater halo to disk mass ratios. In all cases, a spiral perturbation develops initially, but it is a transient phase. In case $M_h/M_d=2$, the spiral phase lasts for about four rotations and is very distinct from the bar phase.

In the cases $M_h/M_d=0.25$, 0.5, 1, the bar strength, as measured by Qt max and $Q2$ max, reaches its greatest value several rotations after the development of the bar and then decreases to an apparent steady state value.

In the case $M_h/M_d=2$, the bar strength still seems to increase at the end of the calculations; the time scale for the growth of the bar is longer in this case. The time scale for the bar strength (Qt) to reach its maximum value is a strong function of M_h/M_d as is apparent in Fig. 12.

It is evident from Fig. 11 that reasonably strong bars persist in all cases for more than twenty rotation times (i.e. $>5\ 10^9$ yr). The maximum strength of the bar (the largest value of Q_t max over the time of the simulation) is an apparent function of the halo to disk mass ratio (Fig. 12).

The angular velocity of the bar (derived directly from the Fourier analysis of the force) is plotted in Fig. 13 as a function of time for the three cases. It is seen that the angular velocity generally decreases with time, i.e., the bars rotate slower as they evolve towards a steady-state. The angular velocity Ω and the $\Omega-k/2$ curve are shown in Fig. 14 as a function of radius at the final epoch in the case $M_h/M_d=1$. These curves are very similar for the other models. Also shown in this figure are the initial and final values of Ω_p. Corotation initially lies at a radius of 13 units and then over the course of bar evolution, it moves beyond the grid radius to about 16.5 units, based upon an extrapolation of the angular velocity. Initially there are no inner resonances, but resonances appear at about $t=7$ rotations (shortly before the

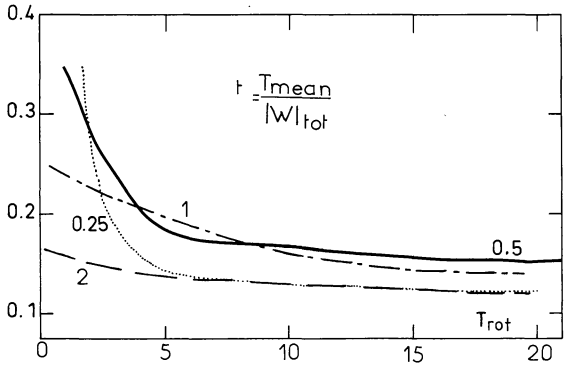

Fig. 15. Estimation of the stability of galaxies, through the ratio t = ratio of mean ordered kinetic energy to total potential energy. According to Ostriker and Peebles (1973) the stability criterium is $t \lesssim 14$

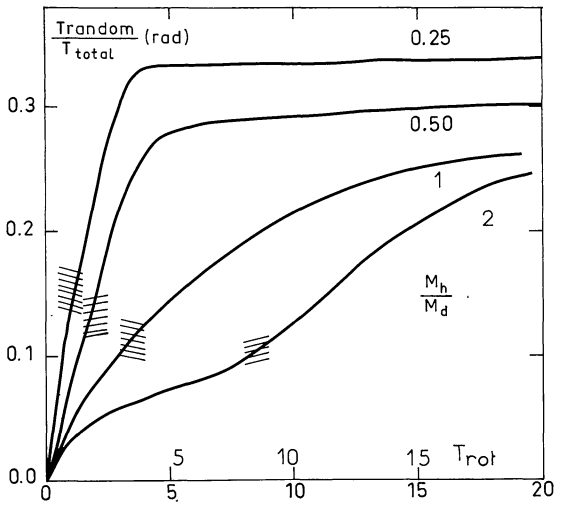

Fig. 16. Evolution of the random kinetic energy in the radial direction in terms of the total kinetic energy, for all models. The appearance of the bar (shaded regions) corresponds to a heating of the systems

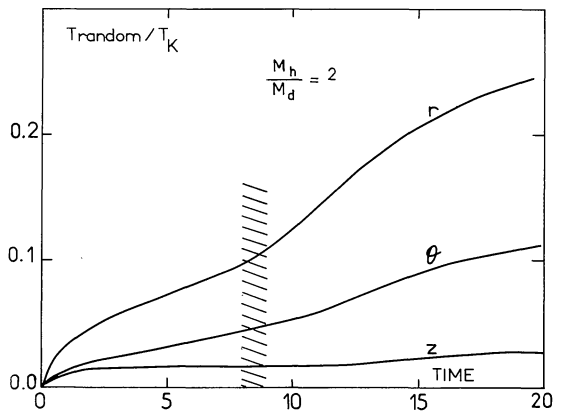

Fig. 17. Evolution of random kinetic energy in the radial, azimuthal and z directions, in terms of the total kinetic energy, for the case $M_h/M_d=2$. The shaded region represents the epoch of formation of the bar. The heating of the system due to the bar is anisotropic

bar reaches its maximum strength); by the end of the simulation there seems to exist two inner resonances at $r=2.5$ and $r=7$ units. However, it should be emphasized that the calculation of $\Omega-k/2$ is based upon a first order expansion about the mean axisymmetric field. When the bar strength becomes larger and particle orbits more elongated this approximation is less accurate and should not be used for the determination of the existence or location of resonances. With the errors of determination of $\Omega-k/2$, it appears that once the bar has become well developed, the bar angular velocity lies near the peak of the $\Omega-k/2$ curve (see Sanders, 1977).

It should be noted that the location of possible resonances is within the bar. If we let r_p be the radius of the peak of $\Omega-k/2$,

$$\frac{r_{\max}}{r_p}=2.2.$$

That is, the maximum tangential force due to the bar occurs well beyond the possible resonances. This also demonstrates that the overall mass distribution is centrally condensed with respect to the bar.

In Fig. 15, the parameter t is plotted for the three cases. This illustrates the decrease of energy in systematic motions (i.e. the heating of the systems) during the dynamical evolution. All systems are initially cold and unstable to the formation of a bar by the Ostriker-Peebles criterion.

In cases $M_h/M_d=0.5, 1$, the rapid development of a bar quickly heats the systems. For the case $M_h/M_d=2$, the longer growth time of the bar leads to a more gradual heating. In case $M_h/M_d=1, 2$, the final value of t is near the Ostriker-Peebles criterium for stability ($t\sim 0.11$) but in the case $M_h/M_d=0.5$, the system is somewhat above this limit ($t=0.16$).

From the plots of t as a function of time, we see that the case $M_h/M_d=2$ is still heating at the end of the calculation, while the other two cases have reached a quasi-steady state. This also apparent from Fig. 16, which is a plot of the kinetic random radial energy in terms of the total kinetic energy as a function of time in the three cases. The importance of the bar in the heating of the system is illustrated by the hatchings which correspond again to the region of bar formation. The lack of continued heating after 10 rotations for $M_h/M_d=0.25, 0.5, 1$, suggests that no further relaxation is going on; in particular, that numerical relaxation is not a significant effect.

The appearance of the bar heats the system in an anisotropic way. This is shown in Fig. 17, where the time evolution of random kinetic energy in all three directions (r, φ, z) is plotted for the case $M_h/M_d=2$. Here the bar appears between 8 and 9 rotations, and the heating due to the bar is unambiguously distinguished from the initial relaxation. This heating only increases the velocity dispersions in the plane (r, φ) and not perpendicular to the plane. This anisotropic heating is similar to that found by Hohl and Zang (1979).

VI. Conclusion

In the present calculations, a purely axisymmetric disk is not obtained for a large range of the halo mass to disk mass ratio: $0.25 \leqq M_h/M_d \leqq 2$. Indeed in all cases the bar structure remains quite strong at the end of twenty rotations, with the maximum tangential force of the order of 25% of the axisymmetric force at the radius of maximum tangential forcing. This is consistent with the observed presence of bar components at some level in many

if not most spiral galaxies (de Vaucouleurs, 1963). It is also evident from the present calculations that non axisymmetric systems evolve on a time scale which is much longer than a dynamical time scale but much shorter than the usual two-body relaxation time. The rate of this evolution depends on the ratio of halo mass to disk mass and systems with a larger fraction of total mass in a halo component evolve more slowly. For example, in the case $M_h/M_d=0.25$, the peak bar stength is reached after only two rotations, while in the case $M_h/M_d=2$,the bar strength is still increasing after 20 rotations (Fig. 11). The general character of evolution is the same in all cases, with the bar strength rising to a maximum and then decreasing; however the peak bar strength and relative variations of the bar strength are much larger for those cases with low halo mass (see Fig. 12). It should be emphasized that bars do weaken after reaching a maximum strength, and the time scale for this weakening is comparable to the bar growth time. The decrease of bar strength is accompanied by the general heating of the system as evidenced by the approach of the Ostriker-Peebles parameter t_{0p} to ~ 0.14. It appears that the bars reach a quasi-stationary state after some time; for example in the case of $M_h/M_d=0.25$, the bar strength after rapidly decreasing by a factor 2 in only three rotations, decreases by only 10% in the final 10 rotations. This continuing dissolution of the quasi-stationary bar, if real, would result in the approach to axial symmetry on a Hubble time (50 rotations) in the cases where $M_h/M_d \leqq 1$. However, this longer time scale weakening may be due to an effective two-body relaxation and remains to be confirmed by long time scale calculations with more particles.

The rapid growth of bar followed by weakening and approach to a quasi-stationary state on the same time scale was qualitatively evident in previous calculations (see Hohl, 1975). The measure of bar strength, Qt, quantitatively demonstrates this effect in the present calculations.

In all cases the formation of the bar is accompanied by the development of an anisotropic velocity distribution. This is most evident in the case $M_h/M_d=2$ because of the long growth time scale of the bar (Fig. 17). This phenomenon is also seen in the calculations of Hohl and Zang (1979). The subsequent heating of the system, during the weakening of the bar is less dramatic, and appears to be more isotropic. In all cases, when the bar has formed, the disk viewed edge-on has the peculiar "box" or "peanut" shaped appearance depending on the angle between the bar and the line of sight (see Fig. 9). This might be due to high order resonances between the bar motion and the z-oscillations of the particles in the disk. These forms are observed in a few edge-on galaxies, for example NGC 128 and NGC 7332, and can be the indication of the existence of a bar.

It is suggested by gas-dynamical calculations that bars observed in SBb galaxies represent strong deviations from axial symmetry ($Qt>0.3$). Such bars are produced in these calculations for $M_h/M_d \leqq 1$ but only for a time short compared to a Hubble time; i.e. for $M_h/M_d \leqq 1$, strong bars appear to be a transient phenomenon. However, in the case $M_h/M_d=2$, the bar strength is still increasing after 20 rotation times, or about one half a Hubble time. This suggests that the bars observed in SBb galaxies have not persisted since the epoch of galaxy formation, but have developed more recently in systems with $M_h/M_d \geqq 2$. It is possibly the rate of global dynamical evolution of non axisymmetric systems which determines whether or not a disk galaxy will now appear as a barred or unbarred galaxy, and this rate of evolution depends strongly on M_h/M_d. Therefore, the fraction of the galactic mass in a hot halo is likely to be a critical parameter in determining the morphology of galaxies. In systems with low M_h/M_d, bars develop rapidly but then weaken leaving a hot disk with a weak oval distortion. In systems with very high M_h/M_d (possibly $M_h/M_d \sim 4$ judging from calculations by James and Sellwood, 1978) the evolution is so long that a stationary bar may not develop in a Hubble time.

References

Birdsall, C.K., Fuss, D.: 1969, *J. Comput. Phys.* **3**, 494
Berman, R.H., Mark, J.W.K.: 1979, *Astron. Astrophys.* **77**, 31
Combes, F.: 1980, unpublished thesis, Paris University
Eggen, O.J., Lynden-Bell, D., Sandage, A.: 1962, *Astrophys. J.* **136**, 748
Freeman, K.C.: 1977, in I.A.U. Symp. no. 77 Structure and Properties of Nearby Galaxies ed. E. M. Berkhuijseh and R. Wielebinski, Boston, Reidel, p. 3
Hockney, R.W., Brownrigg, D.R.K.: 1974, *Monthly Notices Roy. Astron. Soc.* **167**, 351
Hohl, F.: 1972, *J. Comput. Phys.* **9**, 10
Hohl, F.: 1973, *Astrophys. J.* **184**, 353
Hohl, F.: 1975, IAU *Symp.* **69**, 349
Hohl, F.: 1978, *Astron. J.* **83**, 768
Hohl, F., Hockney, R.W.: 1969, *J. Comput. Phys.* **4**, 306
Hohl, F., Zang, T.A.: 1979, *Astron. J.* **84**, 585
James, R.A., Sellwood, J.A.: 1978, *Monthly Notices Roy. Astron. Soc.* **182**, 331
Kalnajs, A.J.: 1972, *Astrophys. J.* **175**, 63
Miller, R.H.: 1978, *Astrophys. J.* **224**, 32
Miller, R.H., Prendergast, K.H., Quirk, W.J.: 1970, *Astrophys. J.* **161**, 90
Miller, R.H., Smith, B.F.: 1979, *Astrophys. J.* **227**, 785
Ostriker, J.P., Peebles, P.J.E.: 1973, *Astrophys. J.* **186**, 467
Ostriker, J.P., Peebles, P.J.E., Yahil, A.: 1974, *Astrophys. J.* **193**, L1
Sandage, A.R.: 1961, The Hubble Atlas of Galaxies, Carnegie Institution of Washington
Sanders, R.H.: 1977, *Astrophys. J.* **217**, 916
Sanders, R.H., Tubbs, A.D.: 1980, *Astrophys. J.* **235**, 803
Sellwood, J.A.: 1979 (preprint)
Spitzer, L.: 1968, Diffuse matter in Space, p. 179
Toomre, A.: 1963, *Astrophys. J.* **138**, 385
Toomre, A.: 1964, *Astrophys. J.* **139**, 1217
de Vaucouleurs, G.: 1963, *Astrophys. J. Suppl.* **8**, 31